Article:
Li, X and Jiang, LH orcid.org/0000-0001-6398-0411 (2019) A critical role of the transient receptor potential melastatin 2 channel in a positive feedback mechanism for reactive oxygen species-induced delayed cell death. Journal of Cellular Physiology, 234 (4). pp. 3647-3660. ISSN 0021-9541

https://doi.org/10.1002/jcp.27134

A critical role of the TRPM2 channel in a positive feedback mechanism for ROS-induced delayed cell death

Xin LI[*] and Lin-Hua JIANG[†]

Sino-UK Joint Laboratory of Brain Function and Injury, Xinxiang Medical University, China; School of Biomedical Sciences, Faculty of Biological Sciences, University of Leeds, UK

[†]Correspondence: Dr Lin-Hua Jiang, School of Biomedical Sciences, Faculty of Biological Sciences, University of Leeds, Woodhouse Lane, Leeds LS2 9JT, UK. Email: l.h.jiang@leeds.ac.uk; Telephone: (+)44 (0)113 3434231.

*Current address: Department of Medicine-Endocrinology, Baylor College of Medicine, Houston, Texas, USA.

Running title: TRPM2 in ROS-induced delayed cell death

Keywords: TRPM2 channel, ROS, Zn^{2+}, delayed cell death

GRANT SUPPORTS

This work was supported in part by National Natural Science Foundation of China (31471118), Henan Provincial Department of Education (16IRTSTHN020), the Disciplinary Group of Psychology and Neuroscience Xinxiang Medical University (2016PN-KFKT-06) and Alzheimer's Research Trust (ART/PPG2009A/2).

ABSTRACT

TRPM2 channel activation by ROS plays a critical role in delayed neuronal cell death responsible for post-ischemia brain damage via altering intracellular Zn^{2+} homeostasis, but a mechanistic understanding is still lacking. Here we showed that H_2O_2 induced neuroblastoma SH-SY5Y cell death with a significant delay, dependently of the TRPM2 channel and increased $[Zn^{2+}]_i$, and therefore used this cell model to investigate the mechanisms underlying ROS-induced TRPM2-mediated delayed cell death. H_2O_2 increased concentration-dependently the $[Zn^{2+}]_i$ and caused lysosomal dysfunction and Zn^{2+} loss and, furthermore, mitochondrial Zn^{2+} accumulation, fragmentation and ROS generation. Such effects were suppressed by preventing PARP-1-dependent TRPM2 channel activation with PJ34 and DPQ, inhibiting the TRPM2 channel with 2-APB and ACA, or chelating Zn^{2+} with TPEN. Bafilomycin-induced lysosomal dysfunction also resulted in mitochondrial Zn^{2+} accumulation, fragmentation and ROS generation that were inhibited by PJ34 or 2-APB, suggesting that these mitochondrial events are TRPM2-dependent and sequela of lysosomal dysfunction. Mitochondrial TRPM2 expression was detected, and exposure to ADPR induced Zn^{2+} uptake in isolated mitochondria, which was prevented by TPEN. H_2O_2-induced delayed cell death was inhibited by apocynin and DPI, NOX inhibitors, GKT137831, a NOX1/4-specific inhibitor, or Gö6983, a PKC inhibitor. Moreover, inhibition of PKC/NOX prevented H_2O_2-induced ROS generation, lysosomal dysfunction and Zn^{2+} release, and mitochondrial Zn^{2+} accumulation, fragmentation and ROS generation. Collectively, these results support a critical role for the TRPM2 channel in coupling PKC/NOX-mediated ROS generation, lysosomal Zn^{2+} release, and mitochondrial Zn^{2+} accumulation and ROS generation to form a vicious positive feedback signalling mechanism for ROS-induced delayed cell death.

1 INTRODUCTION

Brain tissues are vulnerable to damage by reperfusion as well as the initial transient ischemia in patients and rodent models of ischemic stroke (Deb et al., 2010; Doyle et al., 2008; Love, 1999). An early study documented in rodent brains that pyramidal neurons died with a significant delay during reperfusion (Kirino, 1982), and such delayed neuronal cell death has been recognized to be critically responsible for post-ischemia cognitive impairment (Doyle et al., 2008; Kitagawa et al., 1990). Development of post-ischemia therapeutics targeting delayed neuronal cell death is attractive in ameliorating reperfusion-associated cognitive dysfunction. It is long known that generation of excessive reactive oxygen species (ROS) occurs during

reperfusion following transient ischemia when re-oxygenation provides oxygen as a substrate for oxidation reactions (Chan, 2001; Sanderson et al., 2013). Besides ischemic stroke, there is a large volume of evidence to support that generation of excessive ROS or oxidative stress is a major factor in the pathogenesis of neurodegenerative diseases including Alzheimer's and Parkinson's diseases (AD and PD) (Belarbi et al., 2017; Cheignon et al., 2018; Liu et al., 2017; Manoharan et al., 2016).

Disruption of intracellular ionic homeostasis such as Ca^{2+} and Zn^{2+} plays an important role in triggering neuronal cell death, and numerous ion channels have been identified as molecular mechanisms in the regulation of intracellular Ca^{2+} and Zn^{2+} homeostasis and in the induction of delayed neuronal death for post-ischemia brain damage and neurodegeneration (Li et al., 2015; Weilinger et al., 2013). The Ca^{2+}-permeable transient receptor potential melastatin 2 (TRPM2) channel is gated by intracellular ADP-ribose (ADPR) (Perraud et al., 2001; Sano et al., 2001) and exhibits potent activation by ROS that promote generation of ADPR mainly via a poly(ADPR) polymerase (PARP)-1 dependent mechanism (Jiang et al., 2010). An earlier study showed a role of the TRPM2 channel in delayed hippocampal neuronal cell death, determined 24 hr after incubation in normal oxygenated and glucose-containing medium following initial exposure for 2 hr to H_2O_2 or oxygen and glucose deprivation (OGD) (Verma et al., 2012), but the signalling mechanisms underlying such delayed neuronal cell death remained unknown. Several recent studies using transgenic TRPM2-knockout mice provide compelling evidence to support an important role for the TRPM2 channel in mediating delayed neuronal cell death (Gelderblom et al., 2014; Jia et al., 2011; Nakayama et al., 2013; Shimizu et al., 2013; Ye et al., 2014), particularly mediating brain damage by reperfusion after transient ischemia (Alim et al., 2013). Consistently, a more recent study has shown that pharmacological intervention of the TRPM2 channel within a clinically relevant therapeutic window during reperfusion protects against post-ischemia brain damage (Shimizu et al., 2016). All these new findings are exciting in identifying the TRPM2 channel as a promising therapeutic target alleviating post-ischemia brain damage, but a mechanistic understanding of TRPM2-dependent delayed neuronal cell death is still lacking. Recent studies also support causative relationships between the TRPM2 channel activation and AD (Ostapchenko et al., 2015) and PD (Sun et al., 2016). Our recent studies have further revealed positive feedback signalling mechanisms in neuronal and microglial cell death initiated by H_2O_2, Zn^{2+} or $A\beta_{42}$ that are known to promote ROS generation (Syed Mortadza et al., 2017, 2018; Li et al., 2017; Li and Jiang, 2018). Therefore, ROS-induced TRPM2-dependent delayed neuronal cell death may represent a

common neurodegeneration mechanism. The human neuroblastoma SH-SY5Y cell is widely used as a cell model in research of neurodegenerative diseases, particularly PD, thanks to its human origin and dopaminergic function properties (Xicoy et al., 2017). The TRPM2 channel expression in SH-SY5Y cells has been well documented (Bao et al., 2016; Chen et al., 2013; Sun et al., 2016). As shown in a recent study, exposure to H_2O_2 and neurotoxin MPTP (1-methyl-4-phenyl-1,2,3,6-tetrahydropyridine) resulted in TRPM2-dependent cell death in SH-SY5Y cells as well as in dopaminergic neurons (Sun et al., 2016). In the present study, we showed that H_2O_2 induced SH-SY5Y cell death with a striking delay in a TRPM2-dependent manner, which is strongly reminiscent of H_2O_2-induced delayed neuronal cell death. We therefore used SH-SY5Y cells to further investigate the signalling mechanisms underlying ROS-induced TRPM2-dependent delayed cell death. We provide evidence to suggest that the TRPM2 channel works together with multiple molecular mechanisms to form a vicious positive feedback responsible for ROS-induced delayed neuronal cell death. Such findings are useful to better understand neuronal cell death associated with post-ischemic stroke brain damage and neurodegenerative diseases.

2 RESULTS

2.1 H_2O_2 induces TRPM2-dependent delayed cell death

Exposure of SH-SY5Y cells to 100 or even 300 μM H_2O_2 for 2 hr resulted in no immediate cell death, but substantial cell death was detected after cells were cultured in H_2O_2-free medium further 24 hr following the initial 2 hr exposure to H_2O_2 (Fig. 1a-b). Cell death was negligible even at 8 hr after H_2O_2-treated cells were cultured in H_2O_2-free medium (Fig. 1a-b). Consistently, the cell viability immediately after exposure to 100 or 300 μM H_2O_2 for 2 hr was similar to that under control conditions, but markedly reduced following culturing in H_2O_2-free medium further 24 hr (Fig. 1c). These results clearly indicate a significant delay in H_2O_2-induced SH-SY5Y cell death. Recent studies show that the TRPM2 channel expressed in SH-SY5Y cells mediates cell death upon prolonged exposure to H_2O_2 (Chen et al., 2013; Sun et al., 2016). We asked how critical the TRPM2 channel is in mediating H_2O_2-induced delayed cell death. H_2O_2-induced delayed cell death was strongly inhibited by treatment, prior to and during exposure to H_2O_2 and subsequent culturing in H_2O_2-free medium, with 1-10 μM 2-APB or 1 μM ACA (Fig. 1d-e), two different TRPM2 channel inhibitors (Jiang et al., 2010), and also significantly, albeit to less extent, by 1 μM PJ34 or 10-30 μM DPQ (Fig. 1f-g), two inhibitors of PARP-1 that is critically engaged in ROS-induced TRPM2 channel activation

(Jiang et al., 2010). These results are consistent with a previous study showing that treatment with clotrimazle, another TRPM2 channel inhibitor, resulted in significant inhibition of H_2O_2-induced delayed cell death in hippocampal neurons (Verma et al., 2012) and, taken together, provide evidence to support a critical role for the TRPM2 channel in mediating H_2O_2-induced delayed cell death. We performed the following experiments using SH-SY5Y cells to investigate the signalling mechanisms underlying ROS-induced TRPM2-dependent delayed neuronal cell death.

2.2 TRPM2-dependent increase in the $[Zn^{2+}]_i$ is critical in H_2O_2-induced delayed cell death

Ca^{2+} is a ubiquitous intracellular signal regulating diverse cell functions including cell death. It was shown that an increase in the intracellular Ca^{2+} ($[Ca^{2+}]_i$) resulting from extracellular Ca^{2+} influx through the TRPM2 channel is important in ROS-induced neuronal cell death (Kaneko et al., 2006). H_2O_2-induced delayed cell death in SH-SY5Y cells was slightly but significantly reduced in extracellular Ca^{2+}-free solution, supporting a role of TRPM2-mediated Ca^{2+} influx in H_2O_2-induced delayed cell death (Fig. 1h-i). H_2O_2-induced delayed cell death in SH-SY5Y cells was almost completely prevented by treatment with 1 μM TPEN or 1-10 μM clioquinol (Fig. 1h-i), two Zn^{2+} chelators. To further study the role of intracellular Zn^{2+}, we carried out single cell imaging using FluoZin3 to monitor the $[Zn^{2+}]_i$ in SH-SY5Y cells under control conditions and after exposure to H_2O_2. Zn^{2+} is present as discrete puncta in control cells (Fig. 2a), as we have recently reported in hippocampal neurons (Li et al., 2017; Li and Jiang, 2018; Ye et al., 2014). Exposure to 10-300 μM H_2O_2 for 0.5-2 hr led to concentration- and duration-dependent increases in the $[Zn^{2+}]_i$ (supplementary Fig. 1a). As anticipated, such increases in the $[Zn^{2+}]_i$ were abolished by treatment with TPEN. H_2O_2-induced increases in the $[Zn^{2+}]_i$ were also reduced by removal of extracellular Ca^{2+} or prior treatment with PJ34 or 2-APB (supplementary Fig. 1b-c), suggesting a role for TRPM2-mediated Ca^{2+} influx in H_2O_2-induced increase in the $[Zn^{2+}]_i$ in SH-SY5Y cells. All these results together indicate a pivotal role for TRPM2-dependent increase in the $[Zn^{2+}]_i$ in H_2O_2-induced delayed cell death, as we have recently proposed for delayed neuronal cell death during reperfusion following transient ischemia (Ye et al., 2014).

2.3 H_2O_2 increases the $[Zn^{2+}]_i$, depending on lysosomal dysfunction and Zn^{2+} release

To shed light on the mechanisms underpinning TRPM2-dependent change in the intracellular Zn^{2+} homeostasis, we carried out single cell imaging of SH-SY5Y cells in conjunction with

using FluoZin3 and intracellular organelle specific fluorescence markers. A majority of the Zn^{2+} puncta in control cells were co-localized with LysoTracker (Fig. 2a and supplementary Fig. 2a), but not MitoTracker (Fig. 2c and supplementary Fig. 2a) or ER-Tracker (supplementary Fig. 2a), suggesting mainly lysosomal location. Brief exposure to H_2O_2 (30 min) elevated the $[Zn^{2+}]_i$ accompanied with strong loss of the Zn^{2+} puncta and LysoTracker fluorescence, indicative of lysosomal dysfunction (Fig. 2a and supplementary Fig. 2b-c). These effects were almost completely inhibited by prior treatment with PJ34 or 2-APB (Fig. 2a-b). Exposure to H_2O_2 also caused diffused distribution of lysosomal cathepsin (supplementary Fig. 2d), providing further evidence to support lysosomal dysfunction.

2.4 H_2O_2 induces TRPM2-dependent mitochondrial Zn^{2+} uptake, morphological change and ROS generation

While there was almost undetectable mitochondrial Zn^{2+} in SH-SY5Y cells under control conditions (Fig. 3c and supplementary Fig. 2a), exposure to H_2O_2 resulted in strong co-localization of FluoZin3 and MitoTracker (Fig. 2c-d), suggesting occurrence of mitochondrial Zn^{2+} uptake. We used RhodZin3, a mitochondrial Zn^{2+} indicator, to further demonstrate H_2O_2-induced mitochondrial Zn^{2+} uptake (Fig. 2e-f). It is known that increased mitochondrial Zn^{2+} uptake compromises the mitochondrial function (Medvedeva and Weiss, 2014; Thornton and Hagberg, 2015). We therefore examined the effects of H_2O_2 on mitochondria. As illustrated in Fig. 3a, exposure to H_2O_2 resulted in remarkable alterations in the morphology of mitochondria from being typically tubular in control cells to largely fragmented in H_2O_2-treated cells, as evidenced by the changes in form factor and aspect ratio that are widely used in quantitative analysis of mitochondrial morphology (Fig. 3b). H_2O_2-induced mitochondrial Zn^{2+} accumulation and mitochondrial fragmentation in SH-SY5Y cells were prevented by prior treatment with PJ34 or 2-APB (Fig. 3a-b and supplementary Fig. 3). We also used MitoTracker-CMH_2Xros, a fluorescent indicator for mitochondrial ROS, to show that H_2O_2 induced considerable and concentration/duration-dependent increases in mitochondrial ROS generation, which was prohibited by prior treatment with PJ34 or 2-APB as well as with TPEN (Fig. 3d-f and supplementary Fig. 4). These results provide evidence to suggest that H_2O_2-induced TRPM2-dependent mitochondrial Zn^{2+} uptake results in mitochondrial dysfunction and promotes mitochondrial ROS generation in SH-SY5Y cells.

2.5 Bafilomycin-induced lysosomal dysfunction leads to TRPM2-dependent mitochondrial Zn^{2+} accumulation, morphological change and ROS production

We hypothesized that H_2O_2-induced lysosomal dysfunction give rise to subsequent mitochondrial Zn^{2+} accumulation leading to mitochondrial dysfunction and ROS production. To test this, we used bafilomycin, an inhibitor of H^+-ATPase to directly disrupt the lysosomal function (Yoshimori et al., 1991). Brief exposure to 100 nM bafilomycin resulted in mitochondrial Zn^{2+} accumulation (Fig. 4a), fragmentation (Fig. 4c-d and supplementary Fig. 5a-b) and ROS production (Fig. 4e-f and supplementary Fig. 5c-d). Interestingly, these bafilomycin-induced mitochondrial effects were largely inhibited by prior treatment with PJ34 or 2-APB as well as TPEN (Fig. 4). These results support the notion that mitochondrial Zn^{2+} uptake and subsequent mitochondrial dysfunction and ROS generation occur as sequela of bafilomycin/ROS-induced lysosomal dysfunction.

2.6 TRPM2 is located in isolated mitochondria and required for mitochondrial Zn^{2+} accumulation

The inhibition of mitochondrial Zn^{2+} uptake induced by bafilomycin as well as H_2O_2 by PJ34 and 2-APB prompted our attention to the TRPM2 channel with respect to its location in the mitochondria and role in mitochondrial Zn^{2+} uptake in SH-SY5Y cells. While confocal immunofluorescent imaging revealed dispersed subcellular distribution of the TRPM2 protein in SH-SY5Y cells, which exhibited overlapping with MitoTracker in some locations (Fig. 5a), western blotting analysis clearly showed TRPM2 protein in isolated mitochondria from SH-SY5Y cells (Fig. 5b), like in isolated mitochondria from HEK293 cells expressing the TRPM2 channel (Fig. 5b; Li and Jiang, 2018). To demonstrate requirement for the TRPM2 channel in mitochondrial Zn^{2+} accumulation, we imaged Zn^{2+} uptake in isolated mitochondria. Exposure to ADPR significantly increased mitochondrial Zn^{2+} uptake. ADRP-induced mitochondrial Zn^{2+} uptake was only observed in Ca^{2+}-containing, but not Ca^{2+}-free solutions (Fig. 5a), consistent with Ca^{2+} being crucial in ADPR-induced TRPM2 channel activation (Du et al., 2009; Toth and Csanady, 2010). In addition, ADPR-induced mitochondrial Zn^{2+} uptake was prevented by treatment with TPEN (Fig. 5). Taken together, these biochemical and functional results provide consistent evidence to suggest that the TRPM2 channel is located in the mitochondria and required for mitochondrial Zn^{2+} uptake.

2.7 PKC and NAPDH oxidases are engaged in H_2O_2-induced delayed cell death

We next investigated whether in addition to mitochondrial ROS generation, NOX-mediated generation of ROS is involved in H_2O_2-induced delayed cell death in SH-SY5Y cells. H_2O_2-induced delayed cell death was strongly suppressed by prior treatment with 10-30 μM apocynin (Fig. 6a) and 0.1-0.3 μM DPI (Fig. 6b), two generic and structurally distinct NOX inhibitors, and almost completely abolished by prior treatment with 0.1-1 μM GKT137831 (Fig. 6c), a NOX1/4 specific inhibitor. H_2O_2-induced delayed cell death was also prevented by prior treatment with 10-100 nM Gö6983, a PKC inhibitor (Fig. 6d). We used DCFH-DA, a fluorescent indicator for cellular ROS, to further show considerable ROS generation (Fig. 6e-f), which was prevented by prior treatment with apocynin, GKT137831 or Gö6983 (Fig. 6e-f). Moreover, H_2O_2-induced increase in the $[Zn^{2+}]_i$ and lysosomal dysfunction (Fig. 7), mitochondrial Zn^{2+} uptake (Fig. 8a-b), mitochondrial fragmentation (Fig. 8c-d and supplementary Fig. 6), and mitochondrial ROS generation (Fig. 8e-f) were strongly suppressed by prior treatment with apocynin, GKT137831 or Gö6983. Taken together, these results provide clear evidence to support that PKC and NOX, particularly NOX1/4, and NOX-mediated ROS generation are critically engaged in H_2O_2-induced delayed cell death in SH-SY5Y cells.

3 DISCUSSION

The present study demonstrates that H_2O_2 induces delayed cell death in human neuroblastoma SH-SY5Y cells, a cell model widely-used in the study of molecular and signalling mechanisms for neurodegeneration, and provides evidence to suggest that the TRPM2 channel plays a critical role in forming a positive feedback mechanism responsible for ROS-induced delayed cell death (Fig. 9). Such mechanistic insights should be useful for better understanding neuronal cell death associated with post-ischemia brain damage.

It is well-known that excessive ROS is produced during the early stage of reperfusion (Sanderson et al., 2013). Several recent studies provide genetic and pharmacological evidence to support an important role of the ROS-sensitive TRPM2 channel in mediating reperfusion-related brain damage and post-ischemia cognitive dysfunction (Gelderblom et al., 2014; Jia et al., 2011; Nakayama et al., 2013; Shimizu et al., 2016; Shimizu et al., 2013; Verma et al., 2012; Ye et al., 2014). Our recent study further suggests that the TRPM2 channel-dependent increase in the $[Zn^{2+}]_i$ during reperfusion is required for delayed neuronal cell death and post-ischemia brain damage and cognitive dysfunction (Ye et al., 2014). The present study showed that H_2O_2 induced neuroblastoma SH-SY5Y cell death with a prominent delay (Fig. 1a-c), which was

significantly suppressed by treatment with structurally different TRPM2 channel inhibitors (Fig. 1d-e) or PARP-1 inhibitors (Fig. 1e-g). Furthermore, H_2O_2-induced delayed cell death was completely prevented by treatment with structurally different Zn^{2+} chelators (Fig. 1h-k). Overall, the results from the previous and present studies support that activation of the TRPM2 channel plays a critical part in ROS-induced alterations in the intracellular Zn^{2+} homeostasis for delayed neuronal cell death.

Lysosomal Zn^{2+} and lysosomal dysfunction are implicated in ROS-induced neuronal cell death (Hwang et al., 2008; Li et al., 2017). As we have recently described in hippocampal neurons (Li et al., 2017; Li and Jiang, 2018; Ye et al., 2014), the present study showed a low level of intracellular Zn^{2+} in control cells, predominantly in puncta, and further demonstrated a majority of Zn^{2+} were of lysosomal localization (Fig. 2a-b and Fig. 7a). Brief exposure to H_2O_2 increased the $[Zn^{2+}]_i$ that was accompanied with loss of lysosomal Zn^{2+} (Fig. 2a-b). These effects were again similar to those observed in hippocampal neurons (Li et al., 2017; Ye et al., 2014). A previous study reported that the TRPM2 channel is localized in the lysosomes and functions as a Ca^{2+} release channel as well as on the cell surface as a Ca^{2+}-permeable channel in pancreatic β-cells (Lange et al., 2009). Our recent study proposes the lysosomal TRPM2 channel mediates lysosomal Zn^{2+} release in pancreatic β-cells (Manna et al., 2015), but it remains to be determined that the TRPM2 channel is located in the lysosomes and plays a similar role in SH-SY5Y cells. H_2O_2 induced substantial reduction in the LysoTracker fluorescence in SH-SY5Y cells (Fig. 2a-b), as previously reported by us and others in hippocampal neurons (Hwang et al., 2008; Li et al., 2017), and diffused subcellular distribution of lysosomal hydrolase (supplementary Fig. 2d). Therefore, lysosomal dysfunction may be the route for lysosomal Zn^{2+} release. Zn^{2+}-binding metallothionein proteins are well known as a cytosolic Zn^{2+} sink and also represent a rich source for Zn^{2+} under oxidative stress, and such Zn^{2+} source was shown to contribute in mediating ischemic brain damage (Dineley et al., 2005; Qian and Noebels, 2005). In the present study, H_2O_2-induced increase in the $[Zn^{2+}]_i$ was almost completely prevented and lysosomal Zn^{2+} puncta were retained in SH-SY5Y cells treated with PJ34 or 2-APB (Fig. 2a-b), disfavouring the possibility that Zn^{2+} release from metallothionein proteins is a major source for H_2O_2-induced increase in the $[Zn^{2+}]_i$ observed in the present study.

In this study, we also provide evidence to show that exposure to H_2O_2 induced considerable mitochondrial Zn^{2+} accumulation (Fig. 2c-f), fragmentation (Fig. 3a-b) and ROS generation (Fig. 3c-f), all of which were prevented by inhibition of the TRPM2 channel (Fig. 2e-f and Fig. 3a-f). Bafilomycin-induced lysosomal dysfunction was also effective in inducing

mitochondrial Zn^{2+} accumulation, fragmentation and ROS generation (Fig. 4), suggesting that these events occur as sequela of lysosomal dysfunction. Furthermore, bafilomycin/H_2O_2-induced mitochondrial fragmentation and ROS generation were prevented by treatment with TPEN (Fig. 3f and Fig. 4), suggesting that mitochondrial Zn^{2+} accumulation triggers alterations in the mitochondrial function. Bafilomycin-induced mitochondrial events, particularly mitochondrial Zn^{2+} accumulation, were sensitive to inhibition by PJ34 and 2-APB (Fig. 4); such observations were unanticipated and raised the possibility that the TRPM2 channel is localized to the mitochondria and required for mitochondrial Zn^{2+} uptake. A previous study proposed that the TRPC3 channel is located in the mitochondria and plays an important role in mediating mitochondrial Ca^{2+} homeostasis (Feng et al., 2013). The TRPM2 immunoreactivity co-existed with MitoTracker in SH-SY5Y cells (Fig. 5a) and the TRPM2 protein was detected in isolated mitochondria from these cells (Fig. 5b). ADPR significantly raised mitochondrial Zn^{2+} uptake in isolated mitochondria from SH-SY5Y cells (Fig. 5c). Furthermore, consistently with Ca^{2+} being critical in ADPR-induced TRPM2 channel activation (Du et al., 2009; Toth and Csanady, 2010), ADPR-induced Zn^{2+} uptake in isolated mitochondria was only observed in the presence of Ca^{2+} (Fig. 5a-b). Taken together, these results have led us to propose that the TRPM2 channel in the mitochondria plays a critical role in mediating the dynamic lysosome-to-mitochondria Zn^{2+} translocation that in turn induces mitochondrial dysfunction and ROS production (Fig. 9), as reported in our recent study in mouse hippocampal neurons and HEK293 cells expressing the human TRPM2 channel (Li and Jiang, 2018).

NOX-mediated ROS generation is a vital signalling pathway in ROS-induced neuronal cell death (Ma et al., 2017). Consistently, H_2O_2 induced cellular ROS generation and delayed cell death in SH-SY5Y cells were strongly reduced by apocynin and DPI, and completely prevented by GKT137831 as well as Gö6983 (Fig. 5). Inhibition of PKC and NOX further prohibited H_2O_2-induced lysosomal dysfunction and increase in the $[Zn^{2+}]_i$ (Fig. 7), mitochondrial Zn^{2+} uptake (Fig. 8a-b), mitochondrial fragmentation (Fig. 8c-d) and mitochondrial ROS production (Fig. 8e-f). Taken together, the results indicate that exposure to ROS, despite insufficient in causing immediate cell death (Fig.1a-c), can set in motion a vicious positive feedback mechanism inducing mitochondrial and NOX-mediated ROS production that drives cell death with a significant delay (Fig. 9).

In summary, we show that the TRPM2 channel acts as a nexus integrating multiple molecular and signalling mechanisms to form a positive feedback responsible for ROS-induced delayed cell death. Such findings should be useful in facilitating evolution of a mechanistic

understanding of delayed neuronal cell death and oxidative stress-related neurodegeneration, and development of therapeutics to treat ischemic stroke damage and neurodegenerative diseases.

4 METHODS AND MATERIALS

4.1 Cell cultures

SH-SY5Y cells used in this study were kindly provided by Dr JA Sim, University of Manchester, UK and maintained in DMEM/F12 medium (Life Technologies) supplemented with 10% foetal bovine serum (FBS) (Sigma) and 1% MEM non-essential amino acids solution (Invitrogen) at 37°C under 5% CO_2 humidified conditions. Maintenance of human embryonic kidney 293 (HEK293) cells with tetracycline-inducible expression of human TRPM2 (hTRPM2) channel in DMEM/F12 medium supplemented with FBS and induction of TRPM2 channel expression were detailed previously (Mann et al., 2015).

4.2 Measurement of cell death

Cells were seeded at a density of 3.5 x 10^4 per well in clear flat bottom 96-well plates (Sarstedt) 24 hr before use. Cells were treated with H_2O_2 at indicated concentrations for 24 hr. To induce delayed cell death, cells were treated with H_2O_2 for 2 hr and continued to be cultured for indicated durations after H_2O_2-containing medium was replaced with fresh H_2O_2-free medium. In some experiments, inhibitors at indicated concentrations were added for 30 min before and during the whole experiment. Cell death was measured as follows. Cells were incubated in 1 μg/ml propidum iodide (PI) (Sigma) and 1 μM Hoechst 33342 (Cell Signaling Technology) for 30 min. Images were captured using an EVOS® Cell Imaging System (Life Technologies) and the cell counting was performed using ImageJ.

4.3 Cell viability assay

The cell viability was determined using lactate dehydrogenase (LDH) based toxicology assay kits (Sigma) according to the manufacturer's instructions. In brief, after cells were prepared and treated as described above for PI staining, 20 μl culturing medium was transferred from each well into in a fresh 96-well plate, and 40 μl LDH assay mixture was added and incubated for 30 min before the reaction was terminated by adding 6 μl 1 M HCl into each well. The absorbance at 490 nm was measured using a Varioskan Flash microplate reader (Thermo

Scientific) and the absorbance at 690 nm representing the background was also measured and subtracted.

4.4 Single cell confocal imaging

Cells were seeded at a density of 1 x 10^5 per dish in poly-L-lysine coated glass-bottom petri dishes (World Precision Instruments) 24 hr before use. After the medium was removed, cells were rinsed with standard buffer solution (SBS: 130 mM NaCl, 5 mM KCl, 1.2 mM $MgCl_2$, 8 mM glucose, 10 mM HEPES, 1.5 mM $CaCl_2$, pH 7.4), and incubated in SBS containing 1 μM FluoZin3-AM or 3 μM RhodZin3-AM (Life Technologies) and, in some experiments, also 25 nM MitoTracker Red CMX-Ros, 100 nM MitoTracker Green FM, 1 μM LysoTracker Red DND-99 or 1 μM ER-Tracker Red Dye. Dishes were incubated at 37°C for 30 min. Cells were rinsed with SBS and kept in SBS. Inhibitors were added into SBS at indicated concentrations to test their effects on the $[Zn^{2+}]_i$. In some experiments, Ca^{2+}-free SBS (130 mM NaCl, 5 mM KCl, 1.2 mM $MgCl_2$, 8 mM glucose, 10 mM HEPES, 0.4 mM EGTA, pH 7.4) was used. Cells were treated with H_2O_2 at indicated concentrations and durations. Cells were maintained with SBS before images were captured using an inverted Zeiss LSM880 confocal microscope with a 63x objective. Environmental control (temperature and CO_2) was applied during cell imaging. The fluorescence intensity was determined using ImageJ.

4.5 Immunofluorescent confocal imaging

Cells were seeded at a density of 2.5 x 10^4 per well on a 13-mm poly-L-lysine-coated coverslips placed in a 24-well plate (Sarstedt). After gently rinsed with phosphate buffer saline (PBS), cells were incubated in Zamboni's fixative (15% (v/v) picric acid and 5.5% (v/v) formaldehyde in PBS) for 1 hr. The fixed cells were rinsed with PBS, and incubated with blocking solution (10% (v/v) goat serum (Sigma) and 4% (v/v) Triton X-100 (Sigma) in PBS) for 1 hr. For some experiments, cells were incubated in 50 nM MitoTracker Red CMX-Ros for 30 min before cells were fixed. Cells were incubated with primary mouse anti-cathepsin B antibody (1:100; Calbiochem) overnight at 4°C. Cells were washed in PBS and incubated with secondary anti-mouse IgG antibody conjugated with fluorescein isothiocyante-conjugated (Sigma) for 1 hr. Cells were washed with PBS and rinsed in water before mounted with SlowFade Gold Antifade with DAPI (Invitrogen) and kept in 4°C. Images were captured using an inverted Zeiss LSM880 confocal microscope with a 63x objective and analysed using ImageJ.

4.6 Measurements of cellular ROS and mitochondrial ROS

Cellular ROS generation was measured using 2',7'-dichlorofluorescin diacetate (DCFH-DA) (Sigma). Cells were incubated with 3 μM DCFH-DA 30 min before treated with indicated conditions and excess dye were washed by replacing medium with PBS before taking images. Mitochondrial ROS generation was measured using MitoTracker Red CM-H_2Xros according to the manufacturer's instructions. After indicated treatments, cells were incubated in medium containing 100 nM MitoTracker Red CM-H_2Xros for 30 min at 37°C. Medium were replaced with fresh PBS before taking images. Images were captured using an EVOS® Cell Imaging System and the fluorescence intensity was determined using ImageJ.

4.7 *Isolation of mitochondria and measurements of mitochondrial Zn^{2+} uptake*

Mitochondria were isolated from SH-SY5Y cells or hTRPM2-expressing HEK293 cells using Mitochondria Isolation kits according to the manufacturer's instructions (Thermo Scientific). Isolated mitochondria were suspended with SBS containing 1 μM RhodZin3-AM (Life Technologies) and incubated at 37°C for 1 hr, and RhodZin3-AM was removed by centrifugation. Mitochondria suspension was dropped on a glass slide and covered with a coverslip. Images were captured using an inverted LSM700 confocal microscope and the fluorescence intensity was determined using ImageJ.

4.8 *Western blotting*

Isolated mitochondria were lysed at 4°C in radioimmunoprecipitation assay buffer for 30 min. Proteins were separated by electrophoresis on 10% sodium dodecyl sulfate-polyacrylamide gels and transferred onto polyvinylidene difluoride membranes. After incubation with primary rabbit anti-TRPM2 antibody (1:1000; Bethyl) or mouse anti-Cyt-c antibody (1:500; BD Pharmingen) and secondary anti-rabbit or anti-mouse antibodies conjugated to horseradish peroxidase. Proteins were visualized using SuperSignal West Pico PLUS Chemiluminescent Substrates (ThermoFisher).

4.9 Data analysis and presentation

Cell death was determined by expressing the number of PI positive cells as percentage of all cells in the same areas identified by DAPI or Hoechst counterstain. Cell viability was determined by expressing the LDH content as percentage of that released from complete cell lysis induced by 2% Triton X-100 (Berns et al., 2009). Co-localization of two fluorescent

signals was quantified by Pearson's correlation coefficient as previously described (Dunn et al., 2011); the coefficient value varies between 0 and 1, being no and total positive correlation. The morphology of mitochondria was characterized by computer-assisted analysis of aspect ratio and form factor (De Vos et al., 2005; Koopman et al., 2005). Data are presented as mean ± standard error mean, where appropriately. Statistical significance analysis was conducted using analysis of variance with *post-hoc* Tukey test, with significance at the level of $p < 0.05$.

AUTHORS' CONTRIBUTIONS

LHJ and XL designed the study. XL performed the experiments and analyzed the data. LHJ and XL wrote and revised the manuscript.

ACKNOWLEDGMENTS

This work was supported in part by National Natural Science Foundation of China (31471118), Henan Provincial Department of Education (16IRTSTHN020), and Alzheimer's Research Trust (ART/PPG2009A/2). XL was a recipient of University of Leeds and Chinese Scholar Council PhD Scholarship.

CONFLICT OF INTEREST

The authors declare no competing financial interests.

FIGURE LEGENDS

Figure 1 H_2O_2 induces TRPM2-dependent delayed cell death.

(a) Representative images showing PI and Hoechst staining of SH-SY5Y cells under control conditions (CTL), or immediately after exposure to 300 μM H_2O_2 for 2 hr, or after 8 and 24 hr culturing in H_2O_2-free culture following the initial 2 hr exposure to H_2O_2. (**b**) Summary of the mean percentage of PI positive cells from 3 independent experiments. **(c)** Summary of the mean LDH release from cells under indicated conditions, expressed as percentage of that from cells lysed with 2% Triton X-100, from 3 independent experiments. **(d-k)** Representative images showing PI and Hoechst staining (d, f, h, j) and summary of the mean PI positive cells from 3 independent experiments (e, g, i, k) for SH-SY5Y cells treated with indicated inhibitors 30 min before and during 2 hr exposure to H_2O_2 and subsequent culturing in H_2O_2-free medium

for 24 hr. Scale bar is 100 μm. ***, $p < 0.005$ compared with control; †††, $p < 0.005$ compared with cells treated with H_2O_2 alone.

Figure 2 TRPM2 channel in H_2O_2-induced increase in the $[Zn^{2+}]_i$, lysosomal dysfunction and Zn^{2+} release, and mitochondrial Zn^{2+} accumulation.

(a) Representative images showing FluoZin3 and LysoTracker fluorescence, and their co-localization in merged (and enlarged) images in cells under control conditions (CTL), after exposure to 100 μM H_2O_2 for 30 min, or pre-treated with 1 μM PJ34 or 10 μM 2-APB 30 min before exposure to H_2O_2. **(b)** Summary of the mean FluoZin3 and LysoTracker fluorescence intensity (left and middle), and Pearson's coefficient (right) under indicated conditions, from 30-38 cells from 3 independent experiments for each case. **(c)** Representative images showing FluoZin3 and MitoTracker fluorescence, and their co-localization in merged (and enlarged) images in cells control conditions (CTL) or after exposure to 100 μM H_2O_2 for 30 min. **(d)** Summary of the mean FluoZin3 fluorescence intensity (left) and Pearson's coefficient (right) under indicated conditions from 30-35 cells from three independent experiments for each case. **(e)** Representative images showing RhodZin3 fluorescence in cells under control conditions (CTL), after exposure to 100 μM H_2O_2 for 30 min, or pre-treated with 1 μM PJ34 or 10 μM 2-APB 30 min before exposure to H_2O_2. **(f)** Summary of the mean RhodZin3 fluorescence intensity under indicated conditions from 25-30 individual cells in 3 independent experiments for each case. Scale bar is 10 μm. ***, $p < 0.005$ compared to untreated cells; †††, $p < 0.005$ compared with cells treated with H_2O_2 alone.

Figure 3 TRPM2 channel in H_2O_2-induced mitochondrial fragmentation and mitochondrial ROS production.

(a) Representative MitoTracker fluorescence images showing mitochondrial morphology in control cells, cells after exposure to 100 μM H_2O_2 for 30 min, or cells pre-treated with inhibitors for 30 min before exposure to H_2O_2. **(b)** Summary of the mean form factor (left) and aspect ratio (right) of mitochondria in cells treated with indicated conditions from 60-90 cells in 3 independent experiments for each case. **(c)** Representative images showing mitochondrial ROS (MitoROS) generation in control cells, cells after exposure to H_2O_2 or cells pre-treated with PJ34 for 30 min before exposure to H_2O_2. **(d-f)** Summary of the mean MitoROS intensity under indicated conditions from 3 independent experiments. Scale bar is 10 (a) or 100 μm (c).

***, $p < 0.005$ compared with control cells; †, $p < 0.05$ and †††, $p < 0.005$ compared with cells treated with H_2O_2 alone.

Figure 4 TRPM2 channel in bafilomycin-induced mitochondrial fragmentation and mitochondrial ROS production.

(a) Representative time-lapse confocal images showing RhodZin3 fluorescence before and 30 min after exposure to 100 nM bafilomycin in control cells or cells pre-treated with inhibitors 30 min before exposure to bafilomycin. **(b)** Summary of the mean RhodZin3 fluorescence intensity under indicated conditions from 3 independent experiments. **(c)** Representative MitoTracker fluorescence images showing mitochondrial morphology in cells treated by bafilomycin or pre-treated with inhibitors for 30 min before bafilomycin treatment. **(d)** Summary of the mean form factor (top) and aspect ratio (bottom) of mitochondria in cells from 50-60 cells in 3 independent experiments for each case. **(e)** Representative images showing mitochondrial ROS (MitoROS) generation in cells treated by bafilomycin or pre-treated with inhibitors for 30 min prior to bafilomycin treatment. **(f)** Summary of the mean MitoROS generation under indicated conditions from 3 independent experiments. Scale bar is 10 (a, c) or 100 μm (e). *, $p < 0.05$ and ***, $p < 0.005$ compared with control cells; †, $p < 0.05$ and †††, $p < 0.005$ compared with cells treated with bafilomycin alone.

Figure 5 TRPM2 expression and ADPR-induced Zn^{2+} uptake in isolated mitochondria.

(**a**) Representative confocal images showing TRPM2 immunoreactivity (green) and MitoTracker (red) in SH-SY5Y cells. Scale bar is 10 μm. (**b**) Representative western blot showing protein expression of TRPM2 and cytochrome c (Cyt-c), a mitochondrial protein, in mitochondria isolated from SH-SY5Y cells and HEK293 expressing the hTRPM2 channel (TRPM2-HEK293). (**c**) Representative images showing RhodZin3 fluorescence in mitochondria isolated from SH-SY5Y cells, under control conditions (CTL), treatment with 1 mM ADPR 30 min prior to addition of Zn^{2+}, 1 mM ADPR in combination with 1 μM TPEN 30 min prior to addition of Zn^{2+}, or in the absence of Ca^{2+}. Brightfield images showing mitochondria morphology. (**d**) Summary of the mean RhodZin3 fluorescence intensity under indicated condition from 3 independent experiments for each case. *, $p < 0.05$ compared to control; †, $p < 0.05$ and †††, $p < 0.005$ compared to cells treated with Zn^{2+} and ADPR.

Figure 6 PKC and NOX in H_2O_2-induced delayed cell death and ROS generation.

(a-d) *Left*, representative images showing PI staining of SH-SY5Y cells. Cells were exposed to 300 μM H_2O_2 for 2 hr and then cultured H_2O_2-free medium for 24 hr, or were treated with 30 μM apocyinin (a) or 0.3 μM DPI (b) 0.1 μM GKT137831 (c) or 10 nM Gö6983 (d) for 30 min before exposure to H_2O_2. Each panel consists of PI staining image showing dead cells and Hoechst staining image showing all cells. *Right*, summary of the mean percentage of PI positive cells from 3 independent experiments for each case. **(e)** Representative images showing DCFH-DA fluorescence in cells treated by 300 μM H_2O_2 for 2 hr, or cells pre-treated with 30 μM apocyinin, 0.1 μM GKT137831 or 10 nM Gö6983 for 30 min before exposure to H_2O_2. **(f)** Summary of the mean DCFH fluorescence intensity under indicated conditions from 3 independent experiments. Scale bar is 100 μm. ***, $p < 0.005$ compared to control cells; ††, $p < 0.01$ and †††, $p < 0.005$ compared to cells exposed to with H_2O_2 alone.

Figure 7 PKC and NOX in H_2O_2-induced lysosomal dysfunction and Zn^{2+} release.

(a) Representative images showing FluoZin3 and LysoTracker fluorescence and their co-localization in cell under control conditions (CTL), after exposure to H_2O_2 for f 30 min or pre-treated with the inhibitor for 30 min before exposure to H_2O_2. **(b)** Summary of the mean FluoZin3 (top) and LysoTracker fluorescence intensity (middle), and Pearson's coefficient (bottom) under indicated conditions from 20-25 cells from 3 independent experiments for each case. Scale bar is 10 μm (a). *, $p < 0.05$; **, $p < 0.01$ and ***, $p < 0.005$ compared with control cells**.** †, $p < 0.05$ and †††, $p < 0.005$ compared with cells exposed to with H_2O_2 alone.

Figure 8 PKC and NOX in H_2O_2-induced mitochondrial Zn^{2+} accumulation, mitochondrial fragmentation and ROS production.

(a) Representative images showing RhodZin3 fluorescence in control cells (CTL), cells after exposure to 100 μM H_2O_2 for 30 min, or cells pre-treated with indicated inhibitors for 30 min before exposure to H_2O_2. **(b)** Summary of the mean RhodZin3 fluorescence intensity under indicated conditions from 30-35 individual cells in 3 independent experiments for each case. **(c)** Representative MitoTracker fluorescence images showing the mitochondrial morphology in control cells, cells after exposure to 100 μM H_2O_2 for 30 min, or cells pre-treated with the indicated inhibitor for 30 min before exposure to H_2O_2. **(d)** Summary of the mean form factor (left) and aspect ratio (right) of mitochondria in cells under indicated conditions from 40-60 cells in 3 independent experiments for each case. **(e)** Representative images showing mitochondrial ROS (MitoROS) generation in control cells, cells after exposure to 100 μM H_2O_2

for 30 min, or cells pre-treated with indicated inhibitors for 30 min before exposed to H_2O_2. **(f)** Summary of the mean MitoROS under indicated conditions from 3 independent experiments. Scale bar is 10 (a, c) or 100 μm (e). ***, $p < 0.005$ compared with control cells. †††, $p < 0.005$ compared with cells exposed to H_2O_2 alone.

Figure 9 Proposed TRPM2-dependent mechanisms for ROS-induced delayed cell death

Initial exposure to H_2O_2 stimulates protein kinase C (PKC) and NADPH oxidase (NOX) activity and generation of reactive oxygen species (ROS). ROS in turn stimulate PARP-1-mediated production of ADPR and activation of the TRPM2 channel. The TRPM2 channel may mediate lysosomal dysfunction that leads to lysosomal Zn^{2+} release and is required for mitochondrial Zn^{2+} accumulation, triggering mitochondrial dysfunction and ROS generation, which in return enhances NOX-mediated ROS generation and oxidative stress. Such a vicious positive feedback leads to cell death with a significant delay.

REFERENCES

Alim, I., Teves, L., Li, R., Mori, Y., Tymianski, M. (2013). Modulation of NMDAR subunit expression by TRPM2 channels regulates neuronal vulnerability to ischemic cell death. *Journal of Neuroscience, 33*, 17264-17277.

Bao, L., Chen, S.J., Conrad, K., Keefer, K., Abraham, T., Lee, J.P., Wang, J., Zhang, X.Q., Hirschler-Laszkiewicz, I., Wang, H.G., Dovat, S., Gans, B., Madesh, M., Cheung, J.Y., Miller, B.A. (2016). Depletion of the human ion channel TRPM2 in neuroblastoma demonstrates its key role in cell survival through modulation of mitochondrial reactive oxygen species and bioenergetics. *Journal of Biological Chemistry*, *291*, 24449-24464.

Belarbi, K., Cuvelier, E., Destee, A., Gressier, B., Chartier-Harlin, M.C. (2017). NADPH oxidases in Parkinson's disease: a systematic review. *Molecular Neurodegeneration, 12*, 84.

Berns, M., Toennessen, M., Koehne, P., Altmann, R., Obladen, M. (2009). Ibuprofen augments bilirubin toxicity in rat cortical neuronal culture. *Pediatric Research, 65,* 392-396.

Chan, P.H. (2001). Reactive oxygen radicals in signaling and damage in the ischemic brain. *Journal of Cerebral Blood Flow & Metabolism, 21*, 2-14.

Cheignon, C., Tomas, M., Bonnefont-Rousselot, D., Faller, P., Hureau, C., Collin, F. (2018). Oxidative stress and the amyloid beta peptide in Alzheimer's disease. *Redox Biology, 14*, 450-464.

Chen, S.J., Zhang, W., Tong, Q., Conrad, K., Hirschler-Laszkiewicz, I., Bayerl, M., Kim, J.K., Cheung, J.Y., Miller, B.A. (2013). Role of TRPM2 in cell proliferation and susceptibility to oxidative stress. *American Journal of Physiology Cell Physiology, 304*, C548-560.

De Vos, K.J., Allan, V.J., Grierson, A.J., Sheetz, M.P. (2005). Mitochondrial function and actin regulate dynamin-related protein 1-dependent mitochondrial fission. *Current Biology, 15*, 678-683.

Deb, P., Sharma, S., Hassan, K.M. (2010). Pathophysiologic mechanisms of acute ischemic stroke: An overview with emphasis on therapeutic significance beyond thrombolysis. *Pathophysiology, 17*, 197-218.

Dineley, K.E., Richards, L.L., Votyakova, T.V., Reynolds, I.J. (2005). Zinc causes loss of membrane potential and elevates reactive oxygen species in rat brain mitochondria. *Mitochondrion, 5*, 55-65.

Doyle, K.P., Simon, R.P., Stenzel-Poore, M.P. (2008). Mechanisms of ischemic brain damage. *Neuropharmacology, 55*, 310-318.

Du, J., Xie, J., Yue, L. (2009). Intracellular calcium activates TRPM2 and its alternative spliced isoforms. *Proceedings of the National Academy of Sciences of the United States of America, 106*, 7239-7244.

Dunn, K.W., Kamocka, M.M., McDonald, J.H. (2011). A practical guide to evaluating colocalization in biological microscopy. *American Journal of Physiology Cell Physiology, 300*, C723-742.

Feng, S., Li, H., Tai, Y., Huang, J., Su, Y., Abramowitz, J., Zhu, M.X., Birnbaumer, L., Wang, Y. (2013). Canonical transient receptor potential 3 channels regulate mitochondrial calcium uptake. *Proceedings of the National Academy of Sciences of the United States of America, 110*, 11011-11016.

Gelderblom, M., Melzer, N., Schattling, B., Gob, E., Hicking, G., Arunachalam, P., Bittner, S., Ufer, F., Herrmann, A.M., Bernreuther, C., Glatzel, M., Gerloff, C., Kleinschnitz, C., Meuth, S.G., Friese, M.A., Magnus, T. (2014). Transient receptor potential melastatin subfamily member 2 cation channel regulates detrimental immune cell invasion in ischemic stroke. *Stroke, 45*, 3395-3402.

Hwang, J.J., Lee, S.J., Kim, T.Y., Cho, J.H., Koh, J.Y. (2008). Zinc and 4-hydroxy-2-nonenal mediate lysosomal membrane permeabilization induced by H_2O_2 in cultured hippocampal neurons. *Journal of Neuroscience, 28*, 3114-3122.

Jia, J., Verma, S., Nakayama, S., Quillinan, N., Grafe, M.R., Hurn, P.D., Herson, P.S. (2011). Sex differences in neuroprotection provided by inhibition of TRPM2 channels following experimental stroke. *Journal of Cerebral Blood Flow & Metabolism, 31*, 2160-2168.

Jiang, L.H., Yang, W., Zou, J., Beech, D.J. (2010). TRPM2 channel properties, functions and therapeutic potentials. *Expert Opinion on Therapeutic Targets*, *14*,973-988.

Kaneko, S., Kawakami, S., Hara, Y., Wakamori, M., Itoh, E., Minami, T., Takada, Y., Kume, T., Katsuki, H., Mori, Y., Akaike, A. (2006). A critical role of TRPM2 in neuronal cell death by hydrogen peroxide. *Journal of Pharmacological Sciences, 101*, 66-76.

Kirino, T. (1982). Delayed neuronal death in the gerbil hippocampus following ischemia. *Brain Research, 239*, 57-69.

Kitagawa, K., Matsumoto, M., Oda, T., Niinobe, M., Hata, R., Handa, N., Fukunaga, R., Isaka, Y., Kimura, K., Maeda, H, et al. (1990). Free radical generation during brief period of cerebral ischemia may trigger delayed neuronal death. *Neuroscience, 35*, 551-558.

Koopman, W.J., Verkaart, S., Visch, H.J., van der Westhuizen, F.H., Murphy, M.P., van den Heuvel, L.W., Smeitink, J.A., Willems, P.H. (2005). Inhibition of complex I of the electron transport chain causes $O_2^{\cdot-}$ -mediated mitochondrial outgrowth. *American Journal of Physiology Cell Physiology, 288*, C1440-1450.

Lange, I., Yamamoto, S., Partida-Sanchez, S., Mori, Y., Fleig, A., Penner, R. (2009). TRPM2 functions as a lysosomal Ca^{2+}-release channel in beta cells. *Science Signalling, 2*, 71.

Li, C., Meng, L., Li, X., Li, D., Jiang, L,H. (2015). Non-NMDAR neuronal Ca^{2+}-permeable channels in delayed neuronal death and as potential therapeutic targets for ischemic brain damage. *Expert Opinion on Therapeutic Targets, 19*, 879-892.

Li, X., Yang, W., Jiang, L.H. (2017). Alteration in intracellular Zn^{2+} homeostasis as a result of TRPM2 channel activation contributes to ROS-induced hippocampal neuronal death. *Frontiers in Molecular Neuroscience, 10*, 414.

Li, X., Jiang, L.H. (2018). Multiple molecular mechanisms form a positive feedback loop driving amyloid β42 peptide-induced neurotoxicity via activation of the TRPM2 channel in hippocampal neurons. *Cell Death & Disease, 9*, 195

Liu, Z., Zhou, T., Ziegler, A.C., Dimitrion, P., Zuo, L. (2017). Oxidative stress in neurodegenerative diseases: From molecular mechanisms to clinical \pplications. *Oxidative Medicine and Cellular Longevity, 2017*, 2525967.

Love, S. (1999). Oxidative stress in brain ischemia. *Brain Pathology, 9*, 119-131.

Ma, M.W., Wang, J., Zhang, Q., Wang, R., Dhandapani, K.M., Vadlamudi, R.K., Brann, D.W. (2017). NADPH oxidase in brain injury and neurodegenerative disorders. *Molecular Neurodegeneration, 12*, 7.

Manna, P.T., Munsey, T.S., Abuarab, N., Li, F., Asipu, A., Howell, G., Sedo, A., Yang, W., Naylor, J., Beech, D.J., Jiang, L.H., Sivaprasadarao, A. (2015). TRPM2-mediated intracellular Zn^{2+} release triggers pancreatic beta-cell death. *Biochemical Journal, 466*, 537-546.

Manoharan, S., Guillemin, G.J., Abiramasundari, R.S., Essa, M.M., Akbar, M., Akbar, M.D. (2016). The role of reactive oxygen species in the pathogenesis of Alzheimer's disease, Parkinson's disease, and Huntington's disease: A mini review. *Oxidative Medicine and Cellular Longevity, 2016*, 8590578.

Medvedeva, Y.V., Weiss, J.H. (2014). Intramitochondrial Zn^{2+} accumulation via the Ca^{2+} uniporter contributes to acute ischemic neurodegeneration. *Neurobiology of Disease, 68*, 137-144.

Nakayama, S., Vest, R., Traystman, R.J., Herson, P.S. (2013). Sexually dimorphic response of TRPM2 inhibition following cardiac arrest-induced global cerebral ischemia in mice. *Journal of Molecular Neuroscience, 51*, 92-98.

Ostapchenko, V.G., Chen, M.A,, Guzman, M.S., Xie, Y.F., Lavine, N., Fan, J., Beraldo, F.H., Martyn, A.C., Belrose, J.C., Mori, Y., MacDonald, J.F., Prado, V.F., Prado, M.A.M., Jackson, M.F. (2015). The transient receptor potential melastatin 2 (TRPM2) channel contributes to beta-amyloid oligomer-related neurotoxicity and memory impairment. *Journal of Neuroscience, 35*, 15157-15169.

Perraud, A.L., Fleig, A., Dunn, C.A., Bagley, L.A., Launay, P., Schmitz, C., Stokes, A.J., Zhu, Q., Bessman, M.J., Penner, R., Kinet, J.P., Scharenberg, A.M. (2001). ADP-ribose gating of the calcium-permeable LTRPC2 channel revealed by Nudix motif homology. *Nature, 411*, 595-599.

Qian, J., Noebels, J.L. (2005). Visualization of transmitter release with zinc fluorescence detection at the mouse hippocampal mossy fibre synapse. *Journal of Physiology, 566*, 747-758.

Sanderson, T.H., Reynolds, C.A., Kumar, R., Przyklenk, K., Huttemann, M. (2013). Molecular mechanisms of ischemia-reperfusion injury in brain: pivotal role of the mitochondrial membrane potential in reactive oxygen species generation. *Molecular Neurobiology, 47*, 9-23.

Sano, Y., Inamura, K., Miyake, A., Mochizuki, S., Yokoi, H., Matsushime, H., Furuichi, K. (2001). Immunocyte Ca^{2+} influx system mediated by LTRPC2. *Science, 293,* 1327-1330.

Shimizu, T., Dietz, R.M., Cruz-Torres, I., Strnad, F., Garske, A.K., Moreno, M., Venna, V.R., Quillinan, N., Herson, P.S. (2016). Extended therapeutic window of a novel peptide

inhibitor of TRPM2 channels following focal cerebral ischemia. *Experimental Neurology, 283*, 151-156.

Shimizu, T., Macey, T.A., Quillinan, N., Klawitter, J., Perraud, A.L., Traystman, R.J., Herson, P.S. (2013). Androgen and PARP-1 regulation of TRPM2 channels after ischemic injury. *Journal of Cerebral Blood Flow & Metabolism, 33*, 1549-1555.

Sun, Y., Sukumaran, P., Selvaraj, S., Cilz, N.I., Schaar, A., Lei, S., Singh, B.B. (2016). TRPM2 promotes neurotoxin MPP^+/MPTP-induced cell death. *Molecular Neurobiology, 55*, 409-420.

Syed Mortadza, S.A., Sim, J.A., Neubrand, V.E., Jiang, L.H. (2018). A critical role of TRPM2 channel in Aβ42-induced microglial activation and generation of tumor necrosis factor-α. *Glia, 66*, 562-575.

Syed Mortadza, S.A., Sim, J.A., Stacey, M., Jiang, L.H. (2017). Signalling mechanisms mediating Zn^{2+}-induced TRPM2 channel activation and cell death in microglial cells. *Scientific Reports, 7*, 45032.

Thornton, C., Hagberg, H. (2015). Role of mitochondria in apoptotic and necroptotic cell death in the developing brain. *Clinica Chimica Acta, 451*, 35-38

Toth, B., Csanady, L. (2010). Identification of direct and indirect effectors of the transient receptor potential melastatin 2 (TRPM2) cation channel. *Journal of Biological Chemistry, 285*, 30091-30102.

Verma, S., Quillinan, N., Yang, Y.F., Nakayama, S., Cheng, J., Kelley, M.H., Herson, P.S. (2012). TRPM2 channel activation following in vitro ischemia contributes to male hippocampal cell death. *Neuroscience Letters, 530*, 41-46.

Weilinger, N.L., Maslieieva, V., Bialecki, J., Sridharan, S.S., Tang, P.L., Thompson, R.J. (2013). Ionotropic receptors and ion channels in ischemic neuronal death and dysfunction. *Acta Pharmacologica Sinica, 34*, 39-48.

Xicoy, H., Wieringa, B., Martens, G.J. (2017). The SH-SY5Y cell line in Parkinson's disease research: a systematic review. *Molecular Neurodegeneration, 12*, 10.

Ye, M., Yang, W., Ainscough, J.F., Hu, X.P., Li, X., Sedo, A., Zhang, X.H., Zhang, X., Chen, Z., Li, X.M., Beech, D.J., Sivaprasadarao, A., Luo. J.H., Jiang, L.H. (2014). TRPM2 channel deficiency prevents delayed cytosolic Zn^{2+} accumulation and CA1 pyramidal neuronal death after transient global ischemia. *Cell Death & Disease, 5*, e1541.

Yoshimori, T., Yamamoto, A., Moriyama, Y., Futai, M., Tashiro, Y. (1991). Bafilomycin A1, a specific inhibitor of vacuolar-type H^+-ATPase, inhibits acidification and protein degradation in lysosomes of cultured cells. *Journal of Biological Chemistry, 266*, 17707-17712.

Fig. 1

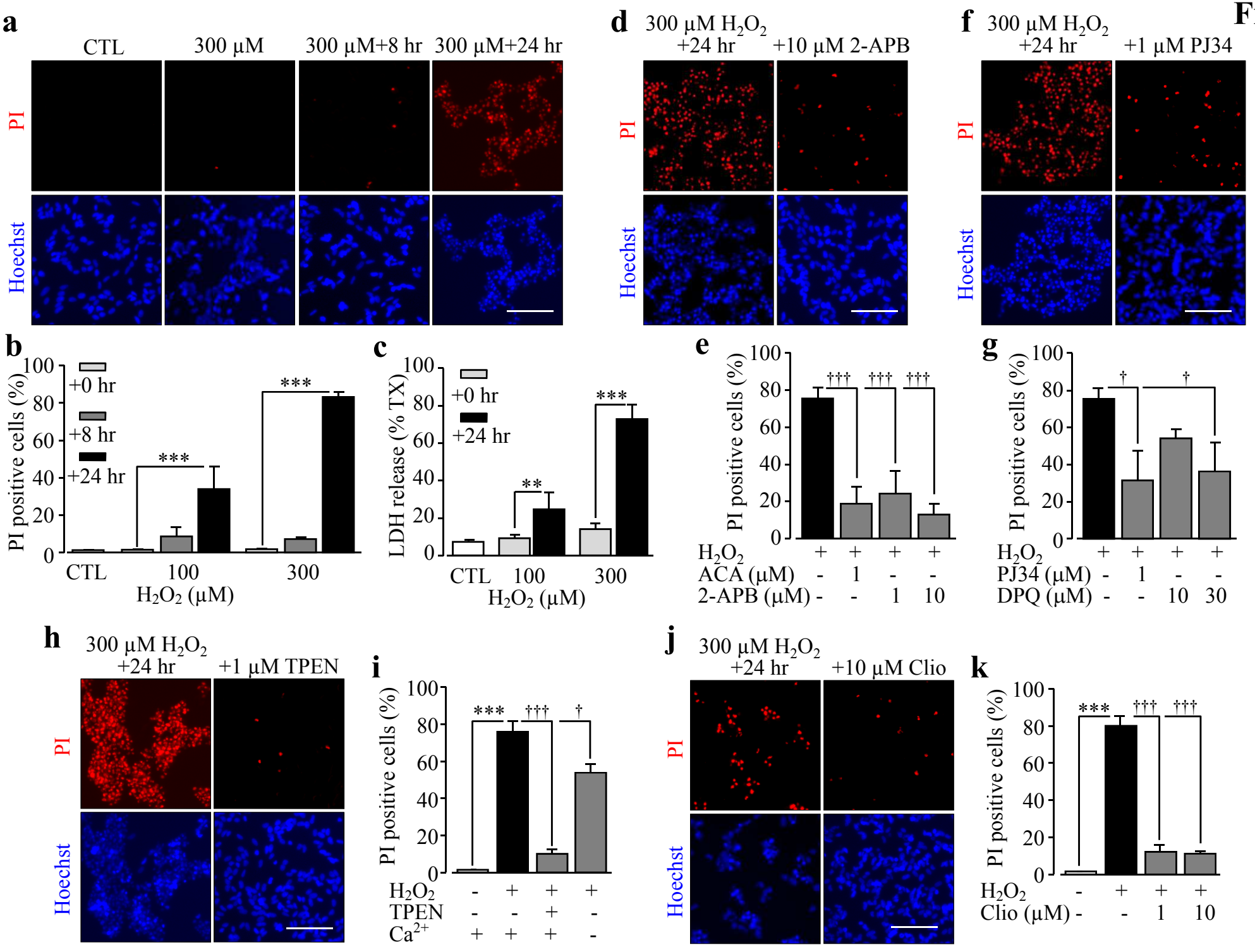
a
CTL
300 μM
300 μM+8 hr
300 μM+24 hr
PI
Hoechst
b
PI positive cells (%)
+0 hr
+8 hr
+24 hr
***
***
CTL
100
300
H2O2 (μM)
c
LDH release (% TX)
+0 hr
+24 hr
**
***
CTL
100
300
H2O2 (μM)
d
300 μM H2O2
+24 hr
+10 μM 2-APB
PI
Hoechst
e
PI positive cells (%)
†††
†††
†††
H2O2 + + + +
ACA (μM) - 1 - -
2-APB (μM) - - 1 10
f
300 μM H2O2
+24 hr
+1 μM PJ34
PI
Hoechst
g
PI positive cells (%)
†
†
H2O2 + + + +
PJ34 (μM) - 1 - -
DPQ (μM) - - 10 30
h
300 μM H2O2
+24 hr
+1 μM TPEN
PI
Hoechst
i
PI positive cells (%)
***
†††
†
H2O2 - + + +
TPEN - - + -
Ca2+ + + + -
j
300 μM H2O2
+24 hr
+10 μM Clio
PI
Hoechst
k
PI positive cells (%)
***
†††
†††
H2O2 - + + +
Clio (μM) - - 1 10

Fig. 2

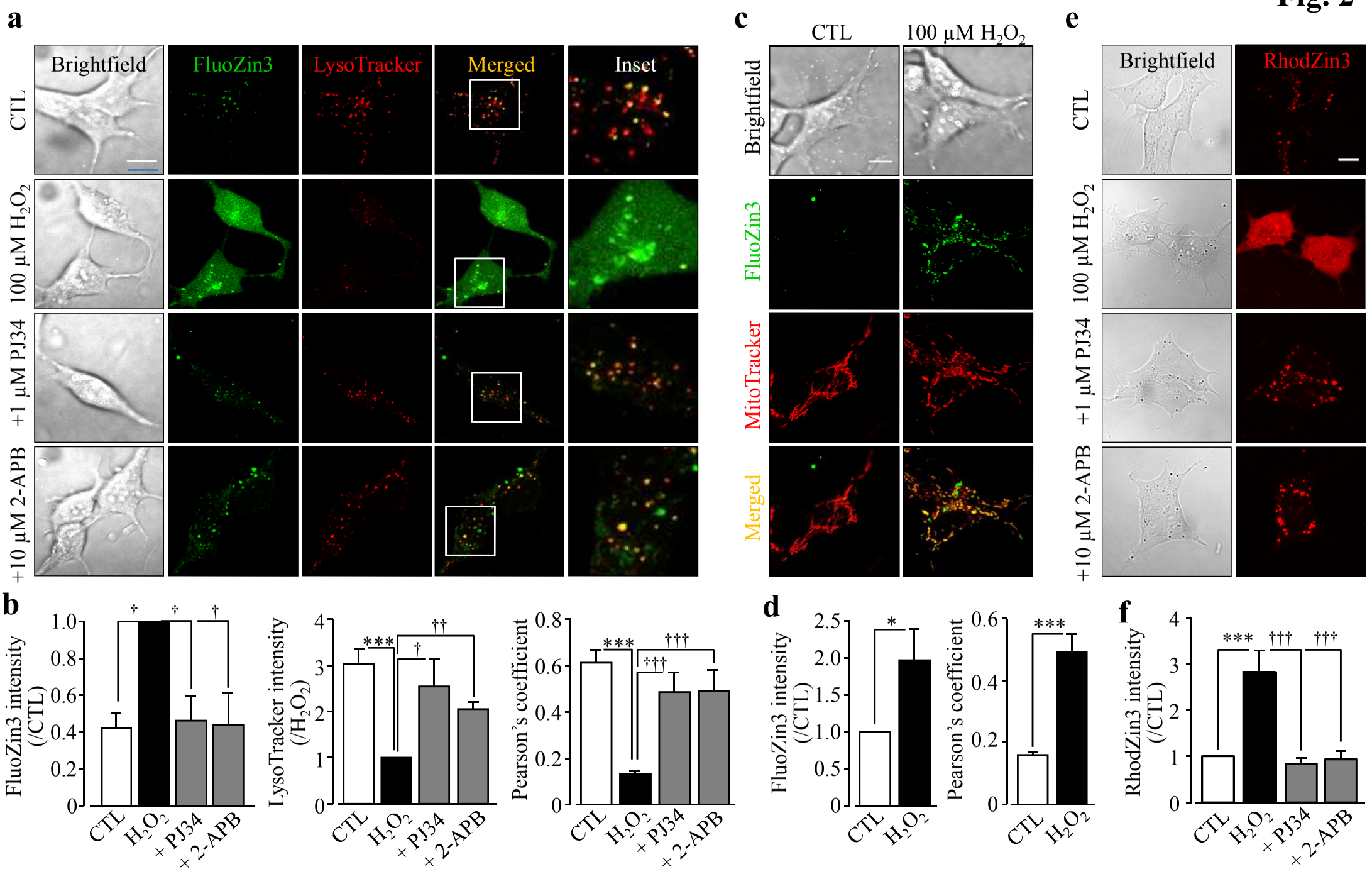
a
Brightfield
FluoZin3
LysoTracker
Merged
Inset
CTL
100 μM H2O2
+1 μM PJ34
+10 μM 2-APB
c
CTL
100 μM H2O2
Brightfield
FluoZin3
MitoTracker
Merged
e
Brightfield
RhodZin3
CTL
100 μM H2O2
+1 μM PJ34
+10 μM 2-APB
b
FluoZin3 intensity (/CTL)
LysoTracker intensity (/H2O2)
Pearson's coefficient
CTL
H2O2
+ PJ34
+ 2-APB
d
FluoZin3 intensity (/CTL)
Pearson's coefficient
CTL
H2O2
f
RhodZin3 intensity (/CTL)
CTL
H2O2
+ PJ34
+ 2-APB

Fig. 3

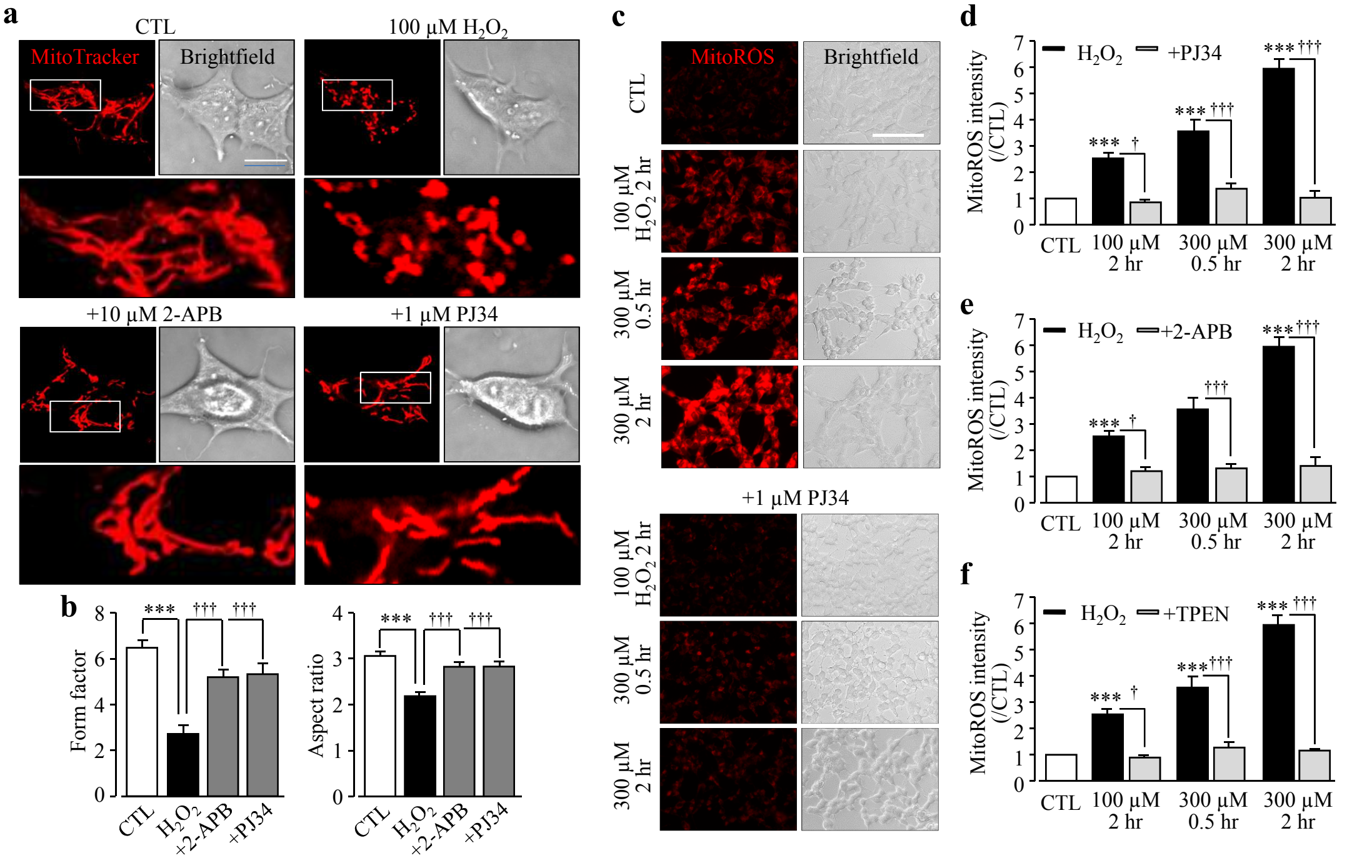
a
CTL
100 μM H2O2
MitoTracker
Brightfield
+10 μM 2-APB
+1 μM PJ34
b
Form factor
Aspect ratio
***
†††
CTL
H2O2
+2-APB
+PJ34
c
MitoROS
Brightfield
CTL
100 μM H2O2 2 hr
300 μM 0.5 hr
300 μM 2 hr
+1 μM PJ34
d
MitoROS intensity (/CTL)
H2O2
+PJ34
100 μM 2 hr
300 μM 0.5 hr
e
+2-APB
f
+TPEN

Fig. 4

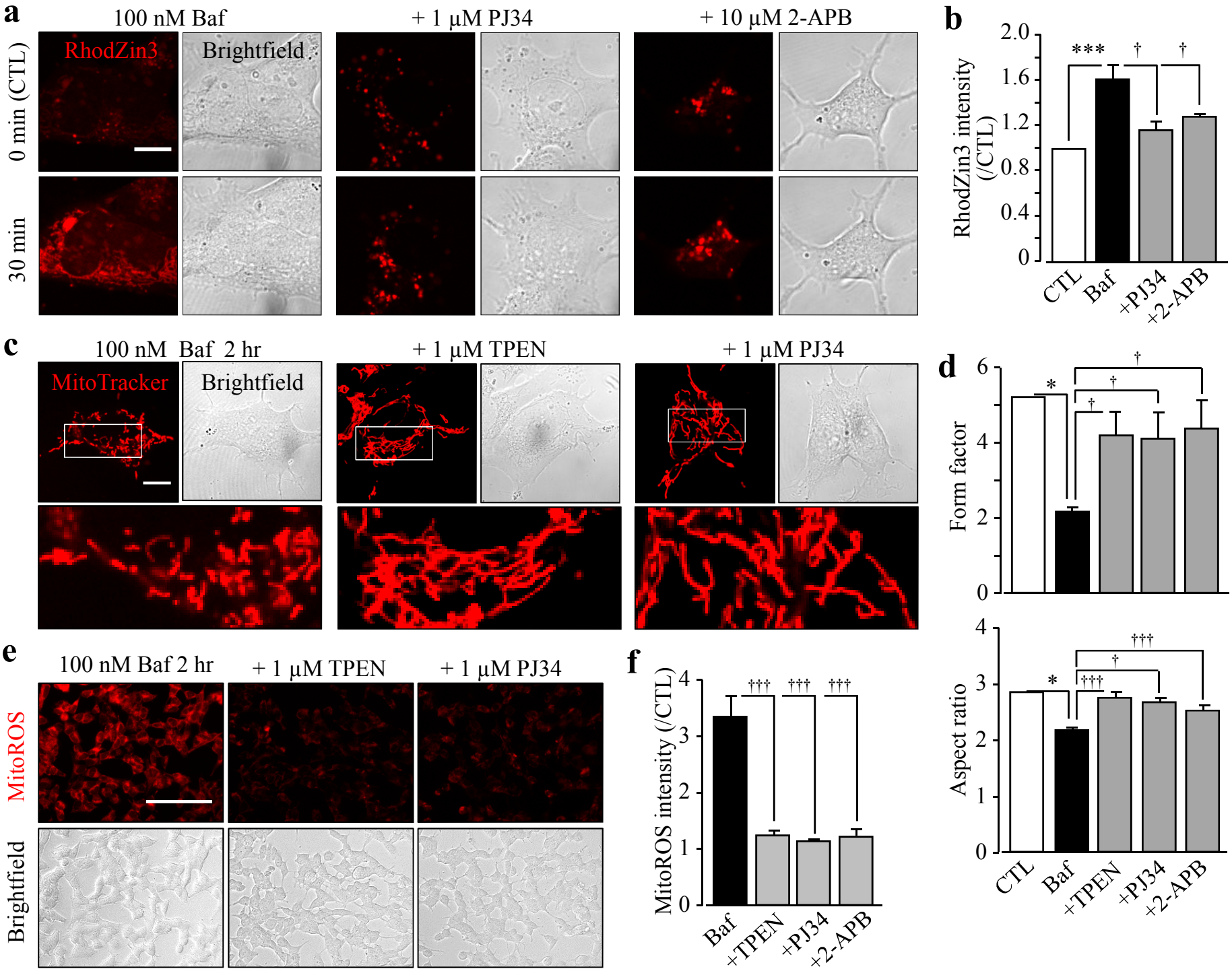
a
100 nM Baf
+ 1 μM PJ34
+ 10 μM 2-APB
RhodZin3
Brightfield
0 min (CTL)
30 min
b
RhodZin3 intensity (/CTL)
2.0
1.6
1.2
0.8
0.4
0
***
†
†
CTL
Baf
+PJ34
+2-APB
c
100 nM Baf 2 hr
+ 1 μM TPEN
+ 1 μM PJ34
MitoTracker
Brightfield
d
Form factor
6
4
2
0
*
†
†
†
Aspect ratio
4
3
2
1
0
*
†††
†
†††
CTL
Baf
+TPEN
+PJ34
+2-APB
e
100 nM Baf 2 hr
+ 1 μM TPEN
+ 1 μM PJ34
MitoROS
Brightfield
f
MitoROS intensity (/CTL)
4
3
2
1
0
†††
†††
†††
Baf
+TPEN
+PJ34
+2-APB

Fig. 5

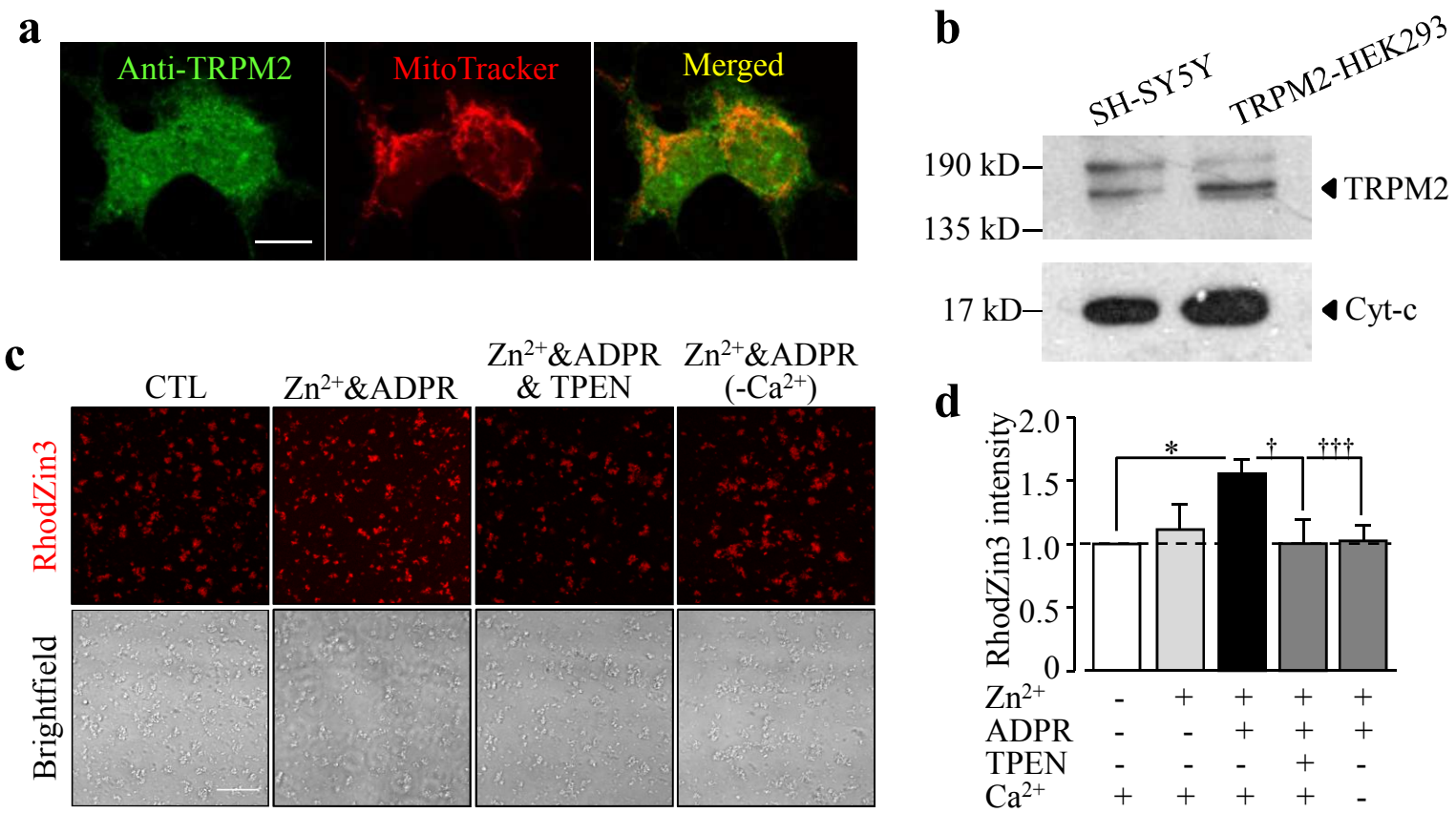
a
Anti-TRPM2
MitoTracker
Merged
b
SH-SY5Y
TRPM2-HEK293
190 kD
135 kD
TRPM2
17 kD
Cyt-c
c
CTL
Zn2+&ADPR
Zn2+&ADPR & TPEN
Zn2+&ADPR (-Ca2+)
RhodZin3
Brightfield
d
RhodZin3 intensity
2.0
1.5
1.0
0.5
0
*
†
†††
Zn2+
ADPR
TPEN
Ca2+

Fig. 6

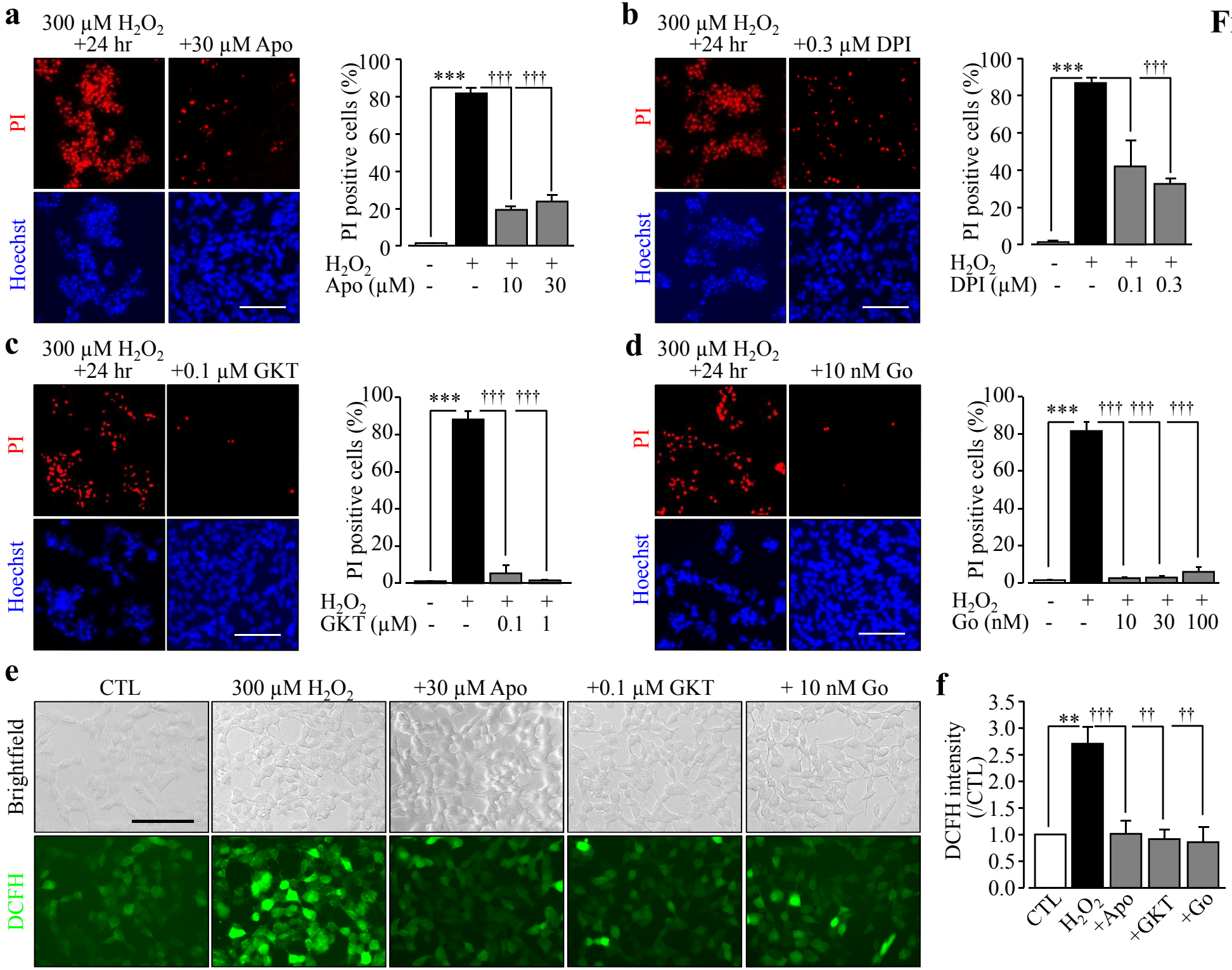
a
300 μM H2O2
+24 hr
+30 μM Apo
PI
Hoechst
PI positive cells (%)
***
†††
H2O2
Apo (μM)
b
+0.3 μM DPI
DPI (μM)
c
+0.1 μM GKT
GKT (μM)
d
+10 nM Go
Go (nM)
e
CTL
+30 μM Apo
+0.1 μM GKT
+ 10 nM Go
Brightfield
DCFH
f
DCFH intensity (/CTL)
**
††
+Apo
+GKT
+Go

Fig. 7

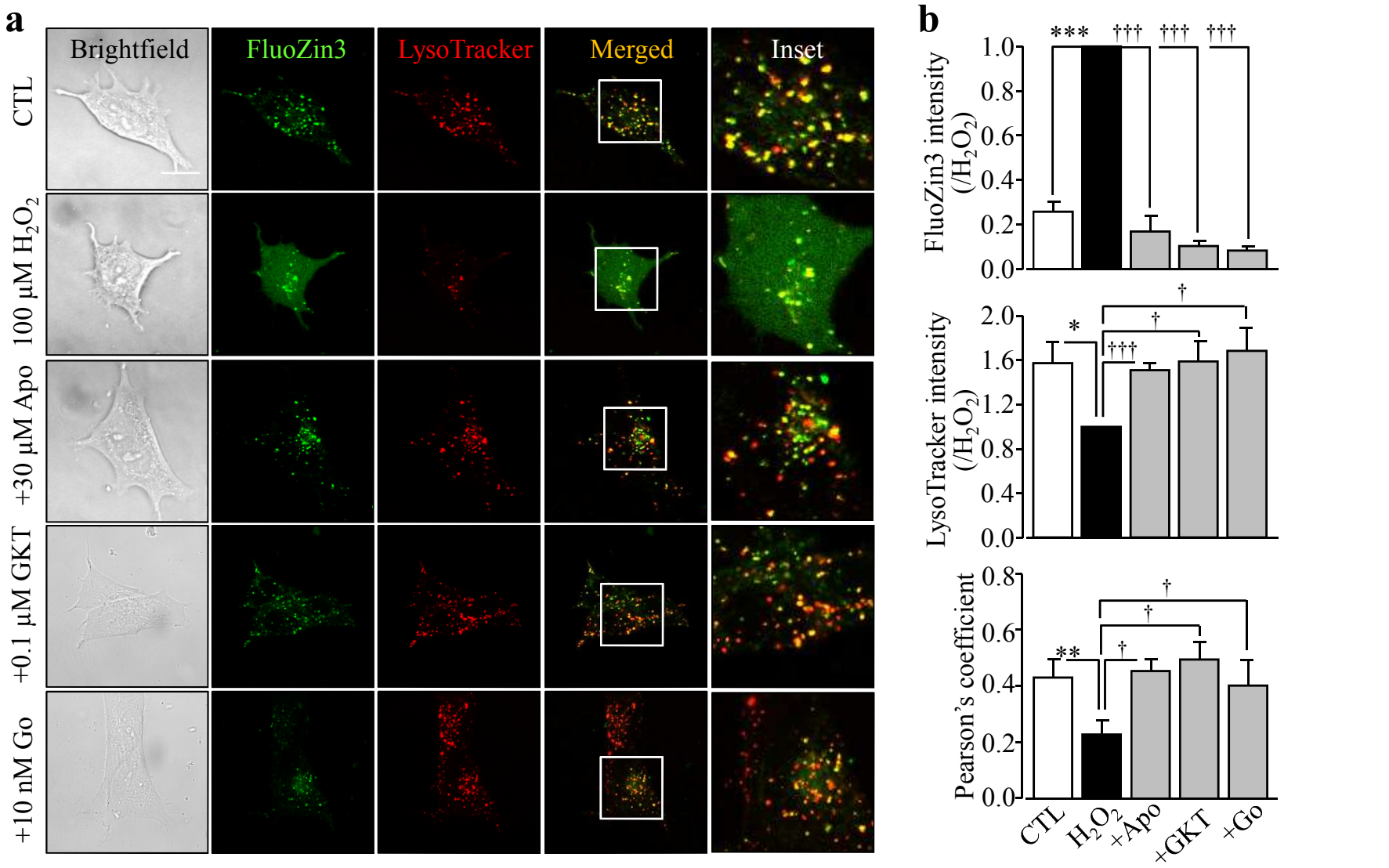
a
Brightfield
FluoZin3
LysoTracker
Merged
Inset
CTL
100 μM H2O2
+30 μM Apo
+0.1 μM GKT
+10 nM Go
b
FluoZin3 intensity (/H2O2)
LysoTracker intensity (/H2O2)
Pearson's coefficient
CTL
H2O2
+Apo
+GKT
+Go

Fig. 8

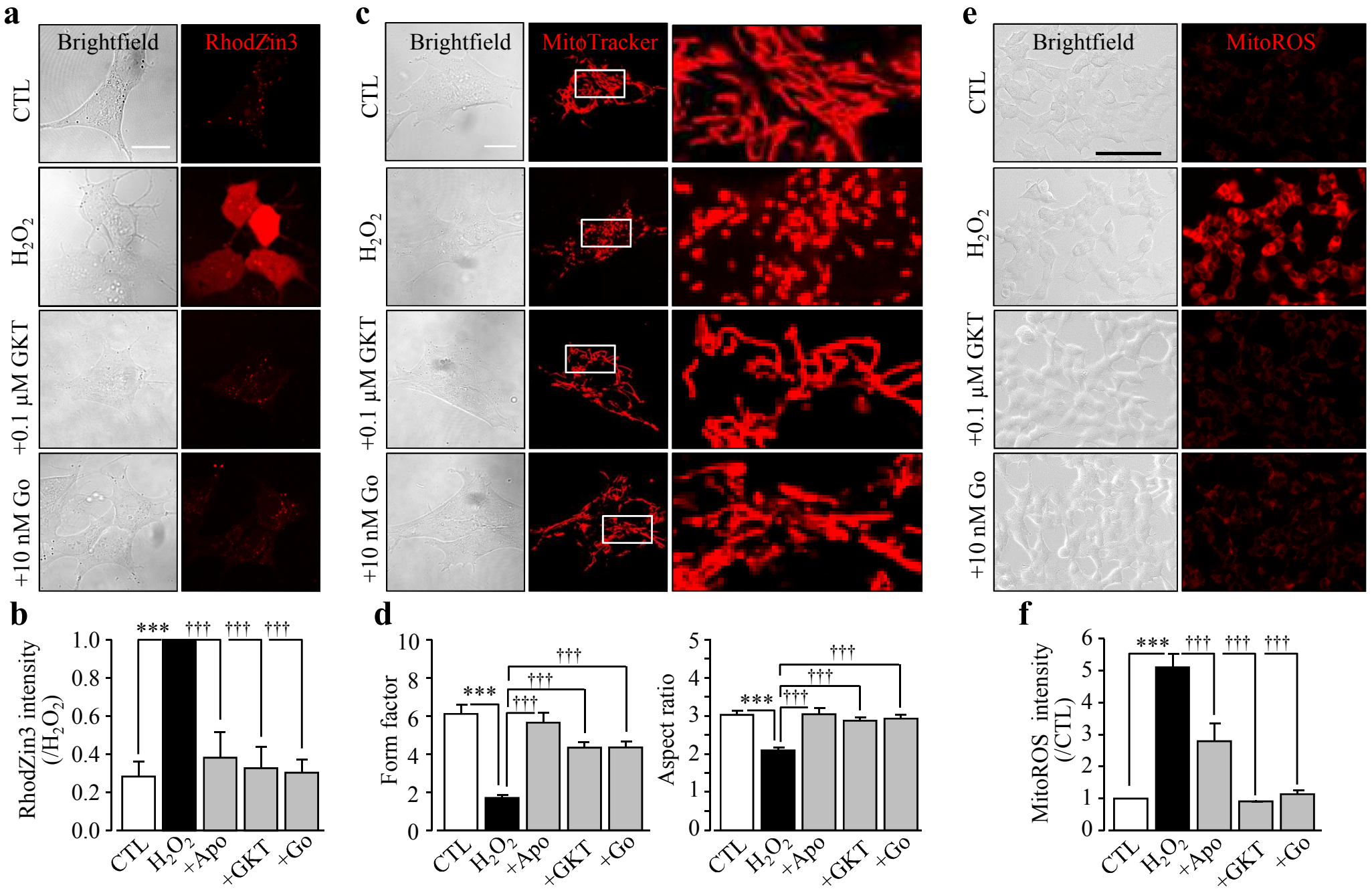
a
Brightfield
RhodZin3
CTL
H2O2
+0.1 μM GKT
+10 nM Go
c
Brightfield
MitoTracker
e
Brightfield
MitoROS
b
RhodZin3 intensity (/H2O2)
***
†††
CTL
H2O2
+Apo
+GKT
+Go
d
Form factor
Aspect ratio
f
MitoROS intensity (/CTL)

Fig. 9

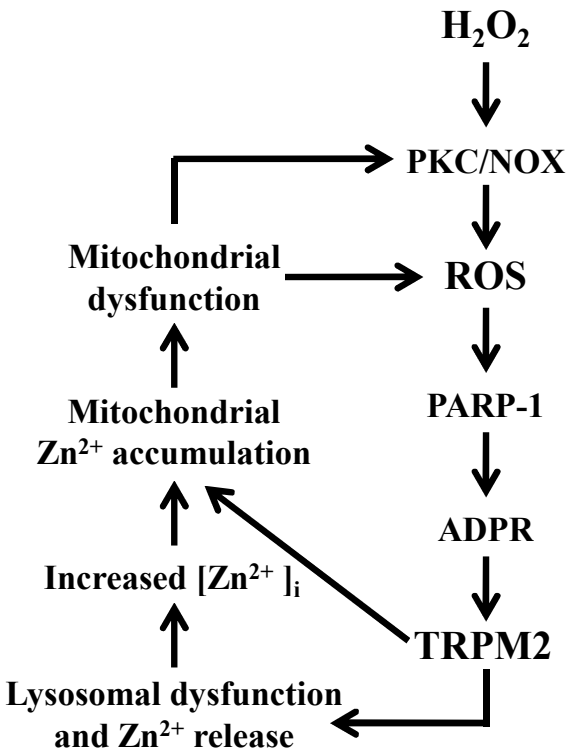
H_2O_2
PKC/NOX
ROS
PARP-1
ADPR
TRPM2
Lysosomal dysfunction and Zn^{2+} release
Increased $[Zn^{2+}]_i$
Mitochondrial Zn^{2+} accumulation
Mitochondrial dysfunction

Graphic summary